

Cite this: *RSC Advances*, 2012, 2, 4135–4151

www.rsc.org/advances

PAPER

MALDI-TOF/TOF CID study of poly(butylene adipate) fragmentation reactions†

Anthony P. Gies,^{‡*a} Sparkle T. Ellison,^{§b} Amit K. Chakraborty,^a Nicholas W. Kwiecien^a and David M. Hercules^a

Received 16th February 2012, Accepted 16th February 2012

DOI: 10.1039/c2ra20283b

This study demonstrates the use of MALDI-TOF/TOF CID fragmentation for the identification of expected and “unexpected” side products in a complex mixture of melt polymerized poly(butylene adipate) (PBA), which aged at room temperature, unexposed to direct sunlight and extreme temperature fluxuations. Expected products include PBA structures terminated with butanediol, adipic acid and buteneol (due to dehydration during synthesis); as well as cyclic architectures with no terminal groups. Additionally, side products were observed containing “unexpected” terminal groups such as glycol, propenyl, methanol, and aldehydes. Low energy fragmentation pathways and computational data are presented to verify the structural assignments of the identified structures, followed by discussion of their probable origin. 1,5-Hydrogen shift reactions were identified as the major low-energy fragmentation pathway.

Introduction

The present study has examined the use of MALDI-TOF/TOF CID fragmentation for the characterization of complex polyester mixtures. The goal of this study was to use CID fragmentation to determine the major degradation pathways for poly(butylene adipate) (PBA) to identify the various end groups and architectures existing within PBA samples. However, it should be noted that the systematic use of MS/MS, as discussed in this study, has significant applications in trouble shooting manufacturing problems, as well as studying structure–property relationships and degradation processes, associated with commercial polymer products.

An earlier MALDI-TOF/TOF CID study of PBA fragmentation¹ reported general mechanistic information that differed from previously reported pyrolysis and TOF-SIMS studies of PBA, and their related urethane polymers.^{2–7} These findings also differed from our previous comparisons between MS/MS and pyrolysis, which showed a direct correlation between the two.^{8–10} The discrepancy appears to have resulted from the higher

collision energy used for the earlier TOF/TOF MS/MS studies (*vide infra*).

The focus of the present paper will be on the mechanisms of PBA fragmentation, learned through MALDI-TOF/TOF CID fragmentation of specific cyclic and linear oligomers, to provide a mechanistic model to explain the products observed in TOF/TOF CID. Particularly important is to identify the lowest energy fragmentation pathways.

Experimental

Materials

Poly(butylene adipate) (PBA) samples were supplied by Bayer Corp. (New Martinsville, WV). These materials were synthesized for earlier MALDI studies to characterize soft- and hard-blocks in polyurethanes.^{11,12} The structure of the polymer repeat unit is that shown in brackets for the species listed in Table 1.

MALDI-TOF/TOF CID measurements

All samples were analyzed using an Applied Biosystems 4700 Proteomics Analyzer MALDI-TOF/TOF MS (Applied Biosystems, Framingham, MA) equipped with a 355 nm Nd:YAG laser. Spectra were obtained in the positive ion mode using an accelerating voltage of 8 kV for the first source, 15 kV for the second source, and a laser intensity approximately 10% greater than threshold. The grid voltage, guide wire voltage, and delay time were optimized for each spectrum to achieve the best signal-to-noise ratio. The CID collision energy is defined by the potential difference between the source acceleration voltage and the floating collision cell; in our experiments this voltage difference was set to 1 kV. Air was used as a collision gas at pressures of 1.5×10^{-6} and 5×10^{-6} Torr (which

^aDepartment of Chemistry, Vanderbilt University, Nashville, TN, 37235, USA. E-mail: APGies@Dow.com; Tel: (979) 238-1778

^bDepartment of Chemistry and Biochemistry, University of South Carolina, Columbia, SC, 29208, USA

† Electronic supplementary information (ESI) available: Details regarding additional PBA CID fragmentation spectra. See DOI: 10.1039/c2ra20283b

‡ Present address is at the Department of Core R&D Analytical Sciences, The Dow Chemical Company, 2301 N. Brazosport Blvd., B-1219, Freeport, TX 77541, USA

§ Present address is at the School of Law, University of Kansas, Lawrence, KS 66045, USA

Table 1 Structural assignments for precursor ion peaks (from Fig. 1) selected for MALDI-TOF/TOF CID fragmentation in Fig. 2–9. Oligomer repeat units (n) are shown, ranging from 2 through 23

Species	Structure (M)	(M+Na) ⁺ (Da)	(M+Li) ⁺ (Da)
1-CyE		423.2 (n = 2) 1023.5 (n = 5) 1223.6 (n = 6) 4025.0 (n = 20)	407.2 (n = 2) 1007.5 (n = 5) 1207.6 (n = 6) 4009.0 (n = 20)
1-E1		513.3 (n = 2) 1113.6 (n = 5) 1313.7 (n = 6) 4715.4 (n = 23)	497.3 (n = 2) 1097.6 (n = 5) 1297.7 (n = 6) 4699.4 (n = 23)
1-E2		441.2 (n = 2) 1041.5 (n = 5) 1241.6 (n = 6) 4043.0 (n = 20)	425.2 (n = 2) 1025.5 (n = 5) 1225.6 (n = 6) 4027.0 (n = 20)
1-E3		569.3 (n = 2) 1169.6 (n = 5) 1369.7 (n = 6) 4771.4 (n = 23)	553.3 (n = 2) 1153.6 (n = 5) 1353.7 (n = 6) 4755.4 (n = 23)
1-E4		485.3 (n = 2) 1085.6 (n = 5) 1285.7 (n = 6) 4687.4 (n = 23)	469.3 (n = 2) 1069.6 (n = 5) 1269.7 (n = 6) 4671.4 (n = 23)
1-E5		583.3 (n = 2) 1183.6 (n = 5) 1383.7 (n = 6) 4785.4 (n = 23)	567.3 (n = 2) 1167.6 (n = 5) 1367.7 (n = 6) 4769.4 (n = 23)
1-E6		495.3 (n = 2) 1095.6 (n = 5) 1295.7 (n = 6) 4697.4 (n = 23)	479.3 (n = 2) 1079.6 (n = 5) 1279.7 (n = 6) 4681.4 (n = 23)
1-E7		541.3 (n = 2) 1141.6 (n = 5) 1341.7 (n = 6) 4743.4 (n = 23)	525.3 (n = 2) 1125.6 (n = 5) 1325.7 (n = 6) 4727.4 (n = 23)
1-E8		527.3 (n = 2) 1127.6 (n = 5) 1327.7 (n = 6) 4729.4 (n = 23)	511.3 (n = 2) 1111.6 (n = 5) 1311.7 (n = 6) 4713.4 (n = 23)

will be referred to as “low” and “high” pressure, respectively). All spectra were acquired in the reflection mode with a mass resolution greater than 3000 fwhm; isotopic resolution was observed throughout the entire mass range detected. External mass calibration was performed using protein standards from a Sequazyme Peptide Mass Standard Kit (Applied Biosystems) and a three-point calibration method using Angiotensin I ($m = 1296.69$ Da), ACTH (clip 1-17) ($m = 2093.09$ Da), and ACTH (clip 18–39) ($m = 2465.20$ Da). Internal mass calibration was subsequently performed using a PEG standard ($M_n = 2000$; Polymer Source, Inc.) to yield monoisotopic mass

accuracy better than $\Delta m = \pm 0.05$ Da. The instrument was calibrated before each measurement to ensure constant experimental conditions.

All samples were run in a dithranol matrix (Aldrich) doped with sodium trifluoroacetate (NaTFA, Aldrich) or lithium trifluoroacetate (LiTFA, Aldrich). All spectra displayed the expected mass shifts for the respective cationizing agent; NaTFA was the reagent of choice for comparison with a previous PBA MS/MS report by Rizzarelli *et al.*¹ However, PBA CID fragmentation spectra displayed the best S/N ratios when

analyzed using LiTFA. The S/N ratio was very important when examining precursor ions having low peak intensities. Comparisons using both cationizing agents will be presented, *vide infra*. Samples were prepared using the dried-droplet method with weight (mg) ratios of 50 : 10 : 1 (dithranol : polymer : NaTFA) in tetrahydrofuran (THF, Fisher). After vortexing the mixture for 30 s, 1 μL of the mixture was pipetted onto the MALDI sample plate and allowed to air dry at room temperature. MS and MS/MS data were processed using the Data Explorer 4.9 software (Applied Biosystems).

ESI-TOF MS measurements

Samples were analyzed using a Waters Synapt G2 High Resolution Mass Spectrometer (Waters Corp., Milford, MA). Mass spectra were obtained in the positive ion mode with the spray tip, nozzle, skimmer, ion guide, and TOF mass analyzer potentials (nozzle temperature $-110\text{ }^{\circ}\text{C}$) optimized to achieve the best signal-to-noise ratio. A curtain of nitrogen drying gas was utilized to assist in the ESI process. All spectra were acquired in the reflectron mode (resolution “V” mode) of the TOF mass spectrometer at mass resolutions greater than 17 000 fwhm; isotopic resolution was observed throughout the entire mass range detected. External mass calibration was performed using sodium formate and a fifteen-point calibration method. Internal mass calibration was subsequently performed using the peptide leu-enkephalin (Tyr-Gly-Gly-Phe-Leu) to yield monoisotopic masses exhibiting a mass accuracy better than $\Delta m = \pm 0.001\text{ Da}$. The instrument was calibrated before each measurement to ensure constant experimental conditions. PBA solutions were initially prepared in THF ($50\text{ }\mu\text{g mL}^{-1}$). To aid in their ionization, a $10\text{ }\mu\text{L}$ of a solution containing 0.1% NaTFA in THF was added to the PBA solutions before introduction into the ESI interface by a Cole-Parmer syringe pump at a flow-rate of $10\text{ }\mu\text{L min}^{-1}$.

Terminology

First, it is necessary to define the nomenclature used for PBA MALDI spectra and fragmentation reactions. Figures, tables, and schemes will show structures and mass peaks labeled according to the following key:

(1) Precursor oligomer ion structures are referenced by the symbol given in the “Species” column of Table 1, *e.g.*, 1-E1, 1-E2, 1-E3, *etc.* Mass values are given in Table 1 for oligomers with 5 and 6 repeat units, for both Na and Li cationization.

(2) Fragment ions are referenced by the symbol given in the “Fragment Series” columns in Table 2 for both Na and Li cationized species. Because PBA conveniently has a repeat unit mass of 200, all members of a structural series will have the same last two digits, but will differ by 200 in the first digit. The symbols “E” for even and “O” for odd will be used to refer to the hundreds digit of a spectral series and the last two digits will be characteristic of the individual fragment series. For example, the Li peak series 225, 425, 625, *etc.* will be referenced as E25; the Li series 351, 551, 751, *etc.* will be referenced as O51

(3) The ion providing the charge will be added at the end of a notation when needed. For example, O53Li^{+} . The symbol “*n*” in a structure refers to the number of polymer repeat units.

Results and discussion

Fig. 1 shows two overall MALDI spectra for the poly(butylene adipate) (PBA) sample used in the present study, for sodium cationization (Fig. 1A) and lithium cationization (Fig. 1B). The most prominent series of peaks is from the linear dibutanol-capped oligomers (1-E1), ranging from 2–39 repeat units, significantly more intense than any other species. This is reasonable given that the PBA sample was prepared for use in polyurethane synthesis. The insets in the range 1000–1320 Da show that the several PBA species seen are independent of the cation used and have approximately the same relative intensities. A total of nine species are observed in the spectra and their proposed structures are given in Table 1, along with the masses of oligomers with $n = 5$ and 6 observed for both lithium and sodium cationization.

Table 3 summarizes the relative ion currents measured for the oligomers of the nine species listed in Table 1, having 4–8 PBA repeat units. The sum of the intensities of all members of a given species (*e.g.*, 1-E1) in the spectrum of each oligomer (*e.g.*, $n = 4$) was measured (for example, 161 relative units for sodiated species 1-E1 in oligomer $n = 4$). The intensities of all nine species so calculated were summed for each oligomer and this was taken as the total ion current for that oligomer (for example, 454 relative units for the sodiated oligomer $n = 4$). The percentages of the ion currents were calculated for each species in the spectrum of each oligomer (*e.g.*, $161/454 = 35\%$ for Species 1-E1 in sodiated oligomer $n = 4$); these are the values shown in Table 3. The ion currents, summed over all oligomers for each species, were used to calculate the overall average relative ion currents shown (rounded) in the column labeled, “Average Percent” The sodium cationized species having the largest relative ion current is butanol–butanol (1-E1) (40%) with cyclic (1-CyE) oligomers being second (19%).

The cyclic oligomers show higher relative intensities for sodium cationization than for lithium (19% *vs.* 14%). Because all measurements were performed on the same sample of polyester, this probably reflects higher polyester affinity for sodium than for lithium. The percent total ion current for 1-CyE decreases with increasing oligomer size, as would be expected. Two species having average percentages between 10 and 20% are butanol-carboxyl (1-E2) and butanol-glycol (1-E4) terminated. The latter probably results from addition of ethylene glycol to the polymerization reaction. The other five species fall into the 1–7% TIC range. The carboxyl-carboxyl (1-E3) oligomers are expected on the basis of synthesis, but the other four are “outliers”: butanol-aldehyde (1-E7), butanol-propyl (1-E5), butanol-butene (1-E6), and butanol-methoxyl (1-E8). Species 1-E3 and 1-E4 are both observed in the electrospray (ESI) spectrum of the PBA sample, so they clearly are synthesis products. Species 1-E5 through 1-E8 are not seen consistently in the ESI spectrum of the PBA sample so one must presume that they most likely are artifacts of the MALDI process.

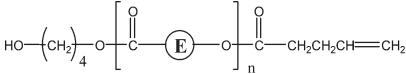
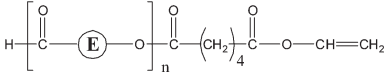
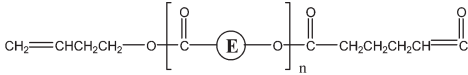
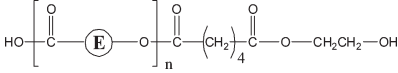
MALDI TOF/TOF of PBA oligomer ions

Di-butanol PBA Precursor (1-E1)—Fig. 2 shows segments of the MALDI-TOF/TOF CID spectra for the di-butanol capped PBA oligomer (1-E1) with $n = 5$. Fig. 2A is for the sodiated species (1113.6 Da) and Fig. 2B is for the lithiated species (1097.6 Da).

Table 2 Structural assignments for fragment peaks in the MALDI-TOF/TOF CID mass spectra reported in Fig. 2–9

Fragment Series		Structure (M)		
Lithium (M + Li) ⁺ (Da)	Sodium (M + Na) ⁺ (Da)	Precursor Species	Fragmentation Mechanism(s)	
2-E07	2-E23	1-CyE, 1-E2, 1-E3	1,5 H-Shift	$\left[\text{C} \left(\begin{array}{c} \text{O} \\ \parallel \\ \text{C} \end{array} \right) (\text{CH}_2)_4 \text{C} \left(\begin{array}{c} \text{O} \\ \parallel \\ \text{C} \end{array} \right) \text{O} (\text{CH}_2)_4 \text{O} \right]_n = \left[\text{C} \left(\begin{array}{c} \text{O} \\ \parallel \\ \text{C} \end{array} \right) \text{E} \text{O} \right]_n$
		1-E1, 1-E4	1,3 H-Shift αH-Acid	$\text{HO} \left[\text{C} \left(\begin{array}{c} \text{O} \\ \parallel \\ \text{C} \end{array} \right) \text{E} \text{O} \right]_n \text{C} \left(\begin{array}{c} \text{O} \\ \parallel \\ \text{C} \end{array} \right) (\text{CH}_2)_4 \text{C} \left(\begin{array}{c} \text{O} \\ \parallel \\ \text{C} \end{array} \right) \text{O} \text{CH}_2\text{CH}_2\text{CH}=\text{CH}_2$
2-E23	2-E39	1-E2, 1-E3, 1-E4	αH-Diol	$\text{HO} (\text{CH}_2)_4 \text{O} \left[\text{C} \left(\begin{array}{c} \text{O} \\ \parallel \\ \text{C} \end{array} \right) \text{E} \text{O} \right]_n \text{C} \left(\begin{array}{c} \text{O} \\ \parallel \\ \text{C} \end{array} \right) \text{CH}_2\text{CH}_2\text{CH}=\text{CH}_2$
2-E25	2-E41	1-E1, 1-E2, 1-E3, 1-E4	1,5 H-Shift 1,3 H-Shift	$\text{HO} \left[\text{C} \left(\begin{array}{c} \text{O} \\ \parallel \\ \text{C} \end{array} \right) \text{E} \text{O} \right]_n \text{C} \left(\begin{array}{c} \text{O} \\ \parallel \\ \text{C} \end{array} \right) (\text{CH}_2)_4 \text{C} \left(\begin{array}{c} \text{O} \\ \parallel \\ \text{C} \end{array} \right) \text{O} \text{CH}_2\text{CH}_2\text{CH}=\text{CH}_2$
2-E51	2-E67	1-E1, 1-E4	1,5 H-Shift αH-Diol	$\text{CH}_2=\text{CH} \text{O} \left[\text{C} \left(\begin{array}{c} \text{O} \\ \parallel \\ \text{C} \end{array} \right) \text{E} \text{O} \right]_n \text{H}$
		1-E4	αH-Diol	$\text{CH}_2=\text{CHCH}_2\text{CH}_2 \text{O} \left[\text{C} \left(\begin{array}{c} \text{O} \\ \parallel \\ \text{C} \end{array} \right) \text{E} \text{O} \right]_n \text{C} \left(\begin{array}{c} \text{O} \\ \parallel \\ \text{C} \end{array} \right) (\text{CH}_2)_4 \text{C} \left(\begin{array}{c} \text{O} \\ \parallel \\ \text{C} \end{array} \right) \text{O} \text{CH}_2\text{CH}_2\text{OH}$
2-E61	2-E77	1-CyE	1,5 H-Shift	$\text{CH}_2=\text{CHCH}_2\text{CH}_2 \text{O} \left[\text{C} \left(\begin{array}{c} \text{O} \\ \parallel \\ \text{C} \end{array} \right) \text{E} \text{O} \right]_n \text{C} \left(\begin{array}{c} \text{O} \\ \parallel \\ \text{C} \end{array} \right) (\text{CH}_2)_4 \text{C} \left(\begin{array}{c} \text{O} \\ \parallel \\ \text{C} \end{array} \right) \text{O} \text{CH}_2\text{CH}_2\text{CH}=\text{CH}_2$
2-E67	2-E83	1-E4	αH-Diol	$\text{O}=\text{CHCH}_2\text{CH}_2\text{CH}_2 \text{O} \left[\text{C} \left(\begin{array}{c} \text{O} \\ \parallel \\ \text{C} \end{array} \right) \text{E} \text{O} \right]_n \text{C} \left(\begin{array}{c} \text{O} \\ \parallel \\ \text{C} \end{array} \right) (\text{CH}_2)_4 \text{C} \left(\begin{array}{c} \text{O} \\ \parallel \\ \text{C} \end{array} \right) \text{O} \text{CH}_2\text{CH}_2\text{OH}$
2-E79	2-E95	1-E1, 1-E2 1-E4	1,5 H-Shift	$\text{CH}_2=\text{CHCH}_2\text{CH}_2 \text{O} \left[\text{C} \left(\begin{array}{c} \text{O} \\ \parallel \\ \text{C} \end{array} \right) \text{E} \text{O} \right]_n \text{H}$
		1-E3	1,3 H-Shift αH-Acid	$\text{HO} \left[\text{C} \left(\begin{array}{c} \text{O} \\ \parallel \\ \text{C} \end{array} \right) \text{E} \text{O} \right]_n \text{C} \left(\begin{array}{c} \text{O} \\ \parallel \\ \text{C} \end{array} \right) \text{CH}=\text{CH}_2$
2-E95	2-O11	1-E1, 1-E2 1-E4	αH-Diol	$\text{O}=\text{CHCH}_2\text{CH}_2\text{CH}_2 \text{O} \left[\text{C} \left(\begin{array}{c} \text{O} \\ \parallel \\ \text{C} \end{array} \right) \text{E} \text{O} \right]_n \text{H}$
2-O23	2-O39	1-E4	αH-Acid	$\text{HO} \text{CH}_2\text{CH}_2 \text{O} \left[\text{C} \left(\begin{array}{c} \text{O} \\ \parallel \\ \text{C} \end{array} \right) \text{E} \text{O} \right]_n \text{C} \left(\begin{array}{c} \text{O} \\ \parallel \\ \text{C} \end{array} \right) \text{CH}=\text{CH}_2$
2-O35	2-O51	1-CyE, 1-E2, 1-E3	1,3 H-Shift αH-Acid	$\text{HO} \left[\text{C} \left(\begin{array}{c} \text{O} \\ \parallel \\ \text{C} \end{array} \right) \text{E} \text{O} \right]_n \text{C} \left(\begin{array}{c} \text{O} \\ \parallel \\ \text{C} \end{array} \right) \text{CH}_2\text{CH}_2\text{CH}=\text{CH}_2$
2-O51	2-O67	1-E1, 1-E2 1-E4	αH-Acid	$\text{HO} (\text{CH}_2)_4 \text{O} \left[\text{C} \left(\begin{array}{c} \text{O} \\ \parallel \\ \text{C} \end{array} \right) \text{E} \text{O} \right]_n \text{C} \left(\begin{array}{c} \text{O} \\ \parallel \\ \text{C} \end{array} \right) \text{CH}=\text{CH}_2$
2-O53	2-O69	1-CyE, 1-E2, 1-E3, 1-E4	1,5 H-Shift, Double 1,5 H-Shift	$\text{HO} \left[\text{C} \left(\begin{array}{c} \text{O} \\ \parallel \\ \text{C} \end{array} \right) \text{E} \text{O} \right]_n \text{C} \left(\begin{array}{c} \text{O} \\ \parallel \\ \text{C} \end{array} \right) (\text{CH}_2)_4 \text{C} \left(\begin{array}{c} \text{O} \\ \parallel \\ \text{C} \end{array} \right) \text{OH}$

Table 2 (Continued)

2-O79	2-O95	1-E4	1,3 H-Shift α H-Acid	
		1-E2, 1-E3	α H-Diol	
2-O89	2-E05	1-CyE	1,3 H-Shift α H-Acid	
2-O97	2-E13	1-E4	1,5 H-Shift	

The two spectra are presented, as was done in Fig. 1, to show the correspondence between Na- and Li-cationization. Side-by-side comparison of Fig. 2A and 2B, identifies a number of advantages for fragmenting lithiated *vs.* sodiated precursor ions: (1) lithiated fragments display more intense peaks in the low mass region under 300 Da—this becomes very useful when fragmenting high mass precursor ions that yield less intense high mass fragments; (2) overall the lithiated CID data present a much “cleaner” spectrum, primarily due to the trace level fragments being shifted to the low mass region and the greater S/N ratios obtained when performing CID fragmentation on lithiated species; and (3) the lithiated spectrum (Fig. 2B) shows higher end group loss of butanol (the peak at 1025.5 Da is the most intense fragment peak in the spectrum)—this aids in the determination of end groups and major degradation pathways.

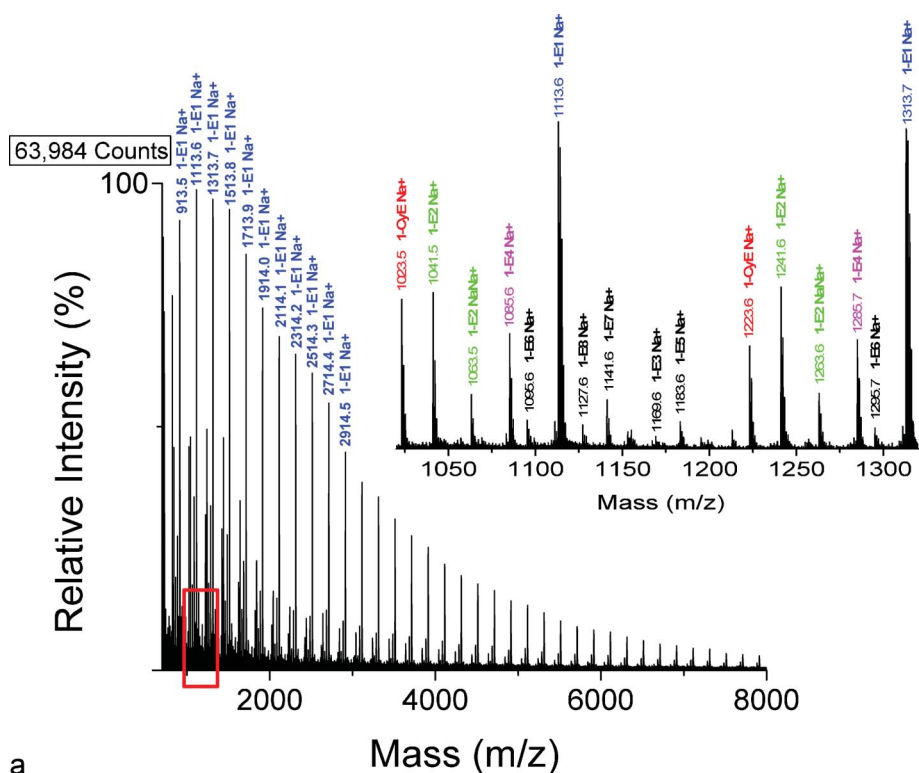
MS/MS spectra of the di-butanol capped oligomers will be used as the general model for PBA fragmentation; MS/MS of oligomers having other end groups will be compared with them. For subsequent discussion, we will consider only lithium cationized spectra because they typically gave better signal-to-noise ratios than their sodium analogs. Depending on the specific oligomer studied, peaks were observed in the MS/MS range from $n = 1$ to $n = 9$.

Fig. 2B shows that two major fragment peak series are observed for Li-cationized di-butanol capped PBA: E25 and E79. PBA preferentially fragments at the C(O)O–CH₂ bond generating butanol-carboxyl (series E25) and butanol-butene (series E79) capped fragments. Table 2 lists the major fragments observed for the di-butanol terminated species, along with their probable structures. The structures are listed alphabetically by the Li spectral series. The parent species that generate a particular fragment series are listed in the “Precursor Species” column for each spectral series. The “Fragmentation Mechanism(s)” column indicates the mechanism by which each species is produced (*vide infra*). Probable fragment ion structures are given in the “Structure” column. The MS/MS peak distributions have their apexes in the 690–850 Da mass region of the CID spectrum. It should be noted that a given spectral series may correspond to more than a single structure; different mechanisms for different parents can produce different structures that are isobars. The E07 series at the top of Table 2 is a good example.

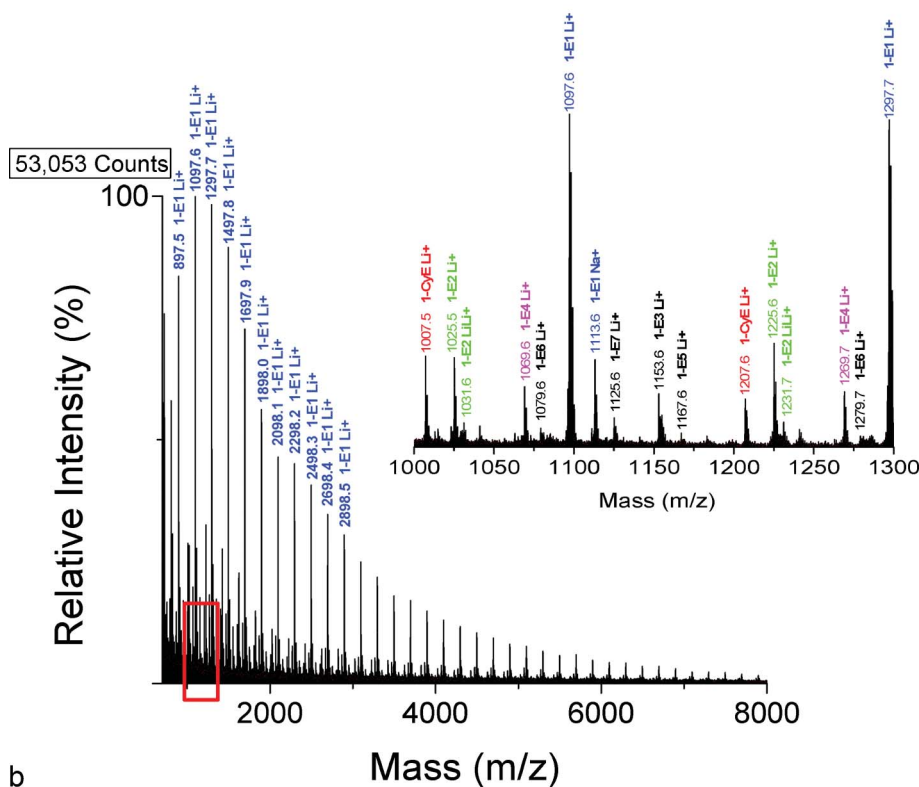
The E25 and E79 fragments result from a single chain fracture involving 1,5 hydrogen transfer (McLafferty Rearrangement) from the diol chain to the ester carbonyl and subsequent fragmentation. This is illustrated for the five major PBA species in Scheme 1. In general, four fragments are possible from 1,5 H-transfer for linear oligomers; they are shown in Scheme 1 as F1, F2, F3, and F4. The mass of a given fragment will be determined by the nature of the end groups (T1 and T2) and where in the chain fracture occurs. Each fragment type will produce a numbered spectral series, as was described earlier; data for the di-butanol oligomers (1-E1) are in the row at the top. Two numbers are given for each F value in Scheme 1. The one on the left is for Li cationization and the one on the right is for Na. There are only two series of peaks possible from 1,5 H-transfer in the di-butanol species because of the symmetry of the di-butanol capped oligomers. So, as shown in Scheme 1, F1 and F4 from lithiated 1-E1 will give E79 species (*e.g.*, 479, 679, 879) and F2 and F3 will give E25 fragment series. It should be noted that 1,5 H-transfer occurs only with hydrogens of the diol segment, not those in the acid segment. As it turns out, this type of 1,5 H-transfer is the major low-energy pathway for all of the PBA parent oligomers (*vide infra*).

Five series of medium and low intensity fragment peak series are observed in the MS/MS of the lithiated parent species 1-E1: E07, E95, O35, O51, and O53. Most of these fragment series can be formed by hydrogen abstraction from a methylene group by one of two possible mechanisms: (1) a 1,3 H-shift to the diol oxygen from the acid α -methylene group or (2) H-abstraction of an α -methylene group by a carbonyl remote from the reaction site. The 1,3 H-shift is illustrated in Scheme 2. The hydrogen transfer causes fragmentation of the C(O)–O bond producing two stable fragments, with a diol terminus on one (E97) and a ketene end group on the other (E07).

Another possibility is that a carbonyl group along the chain, remote from the methylene, abstracts an α -hydrogen from a methylene group even though it is not spatially adjacent to it in the chain. Such a reaction is possible because of the “balled-up” structure of the polymer in the gas phase as will be discussed below. Scheme 3 shows such a process for reaction of the α -methylene group of the acid. The structure shown in the center is the structure after initial H-abstraction; such a radical can fragment by breaking either a C(O)–O or a C–C bond. Each



a



b

Fig. 1 MALDI-TOF mass spectrum of poly(butylene adipate) prepared using a dithranol matrix and cationized with (A) NaTFA or (B) LiTFA. The major peak series are due to 1-E1 oligomers. The inserts cover the mass ranges (A) 1020–1320 Da and (B) 1000–1300 Da, respectively, and indicate species of origin.

fragmentation reaction can produce two series, a stable one (E07 and O51) observed in MS/MS and a radical that is unstable (not observed). This type of hydrogen abstraction appears to be a

major process in the MS/MS of polyesters and will be referred to as “remote hydrogen abstraction.” Such a reaction can also occur with the diol α -methylene hydrogens, producing stable

Table 3 Relative ion currents for PBA oligomers having $n = 4$ –8. Top: sodium cationized. Bottom: lithium cationized. See text for details

Species	Sodium cationized oligomer relative ion current percentages					Average percent
	$n = 4$	$n = 5$	$n = 6$	$n = 7$	$n = 8$	
1-E1	35	40	40	41	45	40
1-CyE	29	22	17	16	13	19
1-E4	9	14	16	16	16	14
1-E2	8	11	12	14	14	12
1-E7	13	6	6	5	5	7
1-E5	2	4	4	4	4	4
1-E6	2	1	2	1	1	1
1-E8	1	1	2	2	1	1
1-E3	1	1	1	1	1	1

Species	Lithium cationized oligomer relative ion current percentages					Average percent
	$n = 4$	$n = 5$	$n = 6$	$n = 7$	$n = 8$	
1-E1	40	48	51	54	54	49
1-CyE	26	15	11	10	8	14
1-E2	13	12	14	15	14	14
1-E4	6	9	9	9	9	8
1-E3	7	7	8	6	7	7
1-E7	3	5	4	3	5	4
1-E8	2	2	1	1	1	1
1-E6	1	1	1	1	1	1
1-E5	2	1	1	1	1	1

series E51 and E95, as shown in Scheme 4. Again, each reaction produces a stable spectral series and an unstable one (not observed). Hypothetically one can generate four stable products for a given oligomer, by α -hydrogen abstraction in Schemes 3 and 4, but only two can occur for Species 1-E1 (and 1-E3) because of the molecular symmetry of di-butanol terminated PBA. In general, remote hydrogen abstraction reactions involving the diol hydrogens are less important than those involving the acid.

Two other series of peaks arise in the MS/MS of Species 1-E1, probably from multiple main-chain fragmentation reactions, to produce fragment series O35 and O53. The ways by which these fragments can be formed are shown in Scheme 5. In both cases there is an initial 1,5 H-transfer from the diol chain to produce a carboxylic acid end group, shown on the left-hand side of the center structure. On the right-hand side one of two hydrogen abstraction reactions occurs. In one case (O53), there is a second 1,5 H-transfer to yield a product terminated by two carboxylic acid groups, shown as the product at the top. In the second case (O35), an α -hydrogen is abstracted from the acid chain (remotely) yielding the product at the bottom with a carboxylic acid group on one end and a ketene on the other, similar to the reaction shown in Scheme 2 for the E07 series. The reactions shown in Scheme 1–5 can account for all of the major peak series (TIC > 1%) observed for di-butanol terminated PBA.

Table 4 shows the ion current distribution among the fragments measured for MS/MS of PBA oligomers for the five major parent species: 1-E1, 1-CyE, 1-E2, 1-E3, and 1-E4. The ion currents shown were calculated using the method of Table 3. The importance of 1,5 H-shift reactions in the MS/MS of di-butanol terminated oligomers (1-E1) is shown in that the E25 and E79 fragments account for about 66% of the total ion current (% TIC) (e.g., 38.5% + 27.7% = 66.2%). Three major fragment series come from remote hydrogen abstraction (O51, E95, and E07) and account for about 29% TIC (12.8% + 9.9% + 5.9% = 28.6%). The two double fragmentations, O35 and O53, account for the remainder. It is noteworthy that the four major fragmentation

reactions from Scheme 1–4 account for 95% TIC for Species 1-E1 oligomers.

Table 5 lists the fragment peak series predicted for MS/MS of the five major oligomers that should be observed for the 1,3 H-shift, α -hydrogen acid chain abstraction, and α -hydrogen diol chain abstraction mechanisms. This allows one to compare the three mechanisms and provides evidence for their occurrence. For the 1-E1 oligomers, the E07 spectral series is predicted by both α -hydrogen acid and 1,3 H-shift mechanisms. However, series O51 is predicted uniquely for α -hydrogen acid chain abstraction, and the E97 series uniquely for the 1,3 H-shift. The O51 series shows 12.8% TIC (Table 4) and the E97 series is not observed, indicating that the 1,3 H-shift reaction plays only a minor role in fragmentation of 1-E1 oligomers. α -Hydrogen diol abstraction predicts both E51 and E95 series, but only the latter is observed. No predictions are provided in Table 5 for 1,3 H-shift reactions from the diol chain for any oligomer, because the series are coincident with those of the 1,5 H-shift mechanism. For this reason, they also were not included in the Table 4 calculations.

It is also interesting to look at how the % TIC of the different fragments varies with oligomer size. The % TIC for E25 and E79 increases with number of repeat units, from ca. 25% each for $n = 4$ to ca. 40% for $n = 10$. This is consistent with 1,5 H-shift being the lowest energy pathway. Conversely, E95 and O51 decrease in % TIC from ca. 20% for $n = 4$ to ca. 6% for $n = 10$, consistent with being higher energy pathways. The other weaker peaks show large statistical intensity variations making it difficult to establish valid trend lines.

Independently of the present work, we have carried out a detailed computational study of PBA oligomers¹³ (ongoing) in which we estimated the ion mobility cross sections for di-butanol terminated PBA tetramers. The method involved first obtaining charge distributions from *ab initio* calculations and then molecular dynamics using a high-temperature sampling protocol. Cooling of cross-sectional snapshots gave a collection of low-energy structures characteristic of the PBA oligomer. A typical

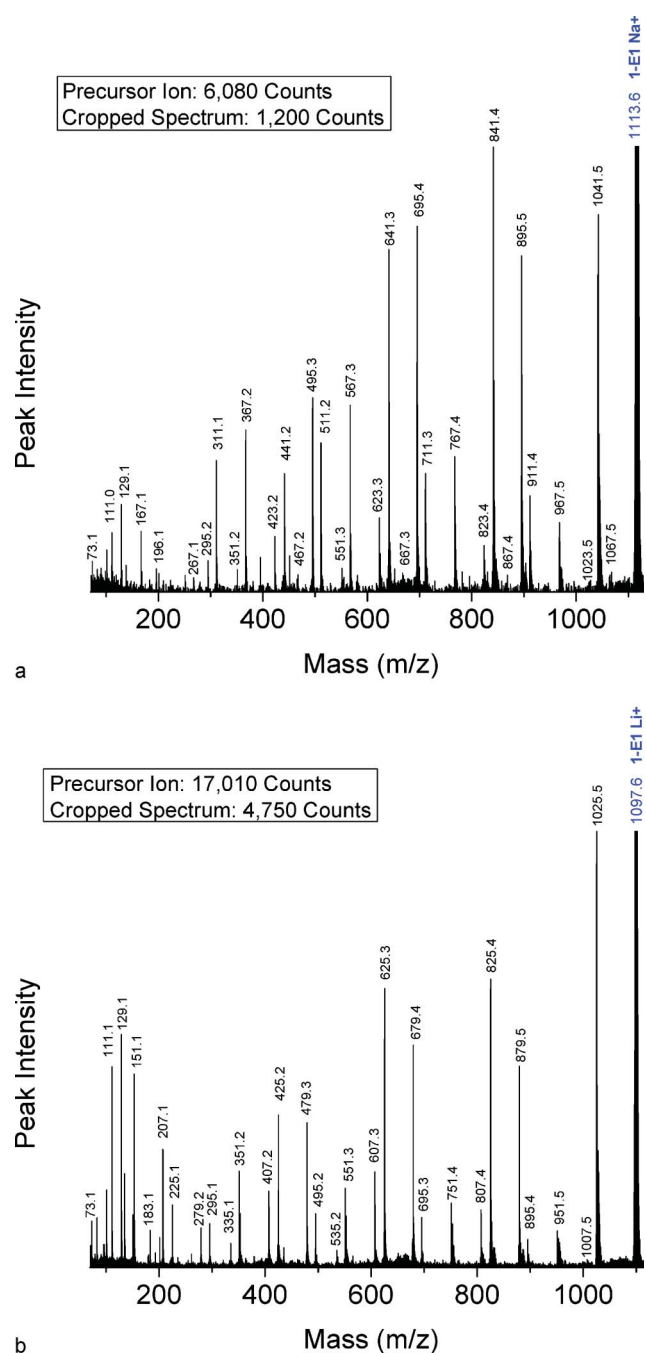


Fig. 2 MALDI-TOF/TOF mass spectrum segment for linear dibutanol terminated PBA structure 1-E1 at a low collision gas pressure of 1.5×10^{-6} Torr. Precursor ions are cationized by (A) Na⁺ (1113.6 Da) or (B) Li⁺ (1097.6 Da).

structure is shown for the sodium cationized di-butanol terminated (Species 1-E1) tetramer in Fig. 3. PBA clearly has a compact structure centered around the sodium ion. This picture confirms that there is a close spatial relationship between carbonyl groups and non-adjacent methylene hydrogens (shown by the green line), supporting the validity of the mechanism of non-adjacent hydrogen transfer to a remote ester carbonyl group as indicated in Scheme 3 and 4.

The next step in our study of the fragmentation of dibutanol-capped PBA (Species 1-E1) was to examine CID fragmentation

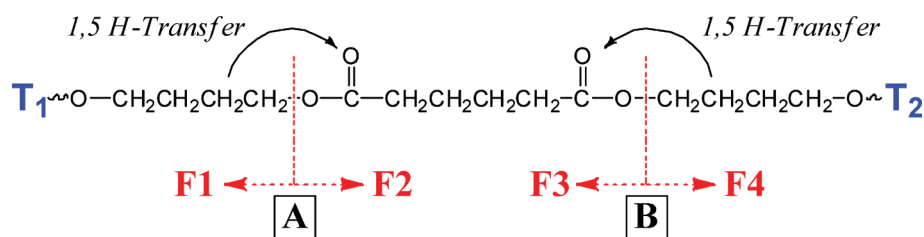
under high and low effective kinetic energy conditions as described in the Experimental section. This should help to further identify the low energy degradation pathways in PBA. To simplify comparison, the high and low energy fragmentation spectra are presented according to mass ranges named for the types of oligomers: (A) monomeric, (B) dimeric/trimeric, (C) tetrameric/pentameric, and (D) hexameric/heptameric.

Focusing on the high energy lithiated CID spectral segments shown in Fig. 4 for the 1-E1 pentamer (1097.6 Da), it is apparent that the monomeric region (Fig. 4A) is primarily composed of small fragments from multiple chain breaks, many having an intrinsic charge; structures are shown in Table 6. Therefore, the most useful data lie in the higher mass dimeric/trimeric region (Fig. 4B). Inspection of the segment shown in Fig. 4B confirms that fragments E25 and E79 (1,5 H-shift) are the *major* species; fragments E07, and O51 (acid chain) are the *medium* species; fragments E95 (diol chain) and O53 (double 1,5 H-shift) are the *small* species; and other species are at the trace level.

Consider the fragmentation pattern of the 1-E1 nanomer generated under low energy CID conditions shown in Fig. 5 (1898.0 Da). The monomeric region (Fig. 5A) shows primarily multi-chain fragments as above. The MS/MS segment shown in Fig. 5B reveals the following: (1) fragments E25 and E79 are the *major* series; (2) fragment E07 is the lone *medium* series; (3) fragments O53 and O35 are *small* series; and (4) others are *trace* series. The next higher mass region, tetrameric through pentameric (Fig. 5C), shows similar distributions of fragment series except for a slight decrease in the intensity of the E07 fragments and series O53 and O35 are at the *trace* level. This same overall trend is shown further in the hexameric through heptameric mass region in Fig. 5D; only fragment series E25 and E79 (1,5 H-shift) show major intensity.

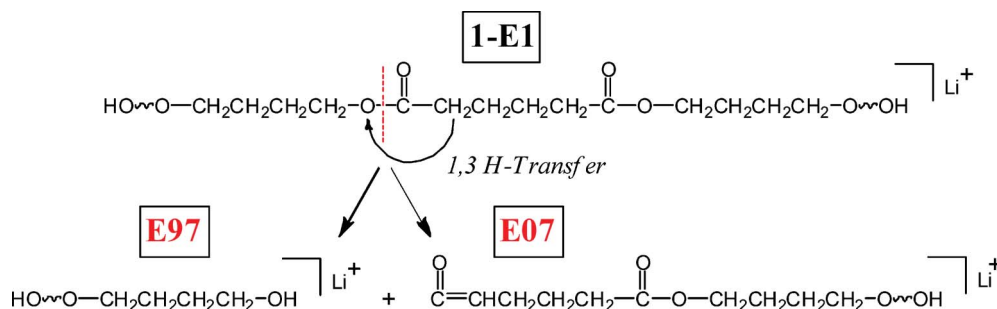
Inspection of the overall peak intensity distributions observed under high and low kinetic energy conditions identify several points of interest. Fig. 4 and 5 support the identification of a 1,5 H-shift (Scheme 1) as the predominant low-energy fragmentation pathway, with E25 and E79 as the major series. As one goes to lower energy scenarios (lower pressure and higher mass oligomers) series E25 and E79 increasingly dominate the spectrum as seen in Fig. 5D. The three minor series shown in Scheme 3 and 4, O51, E07, and E95, are most prominent in spectra obtained under higher energy conditions as in Fig. 4. Similarly, the series involving two H-transfers (Scheme 4), O53 and O35, are most prominent under high energy conditions (Fig. 4B) and are missing under low energy conditions (Fig. 5D). Based on the above, it can be concluded that the 1,5 H-shift reactions represent the lowest energy pathway in the decomposition of poly(butylene adipate).

It is instructive to look at structures for the low-mass fragments produced in PBA MS/MS, as shown in Table 6. The three structures shown at the top of the table are lithium cationized species, whereas the seven below them have intrinsic charge (as shown by lack of a mass shift between Li- and Na-cationized spectra). Two of the lithium fragments are low mass members of more extensive fragment series (O51 and O53) while the third is the only member seen of what would be an O93 series. All but one of the intrinsically charged series correspond to structures having charged carbonyl end groups and probably result from charge-site induced fragmentation based on the

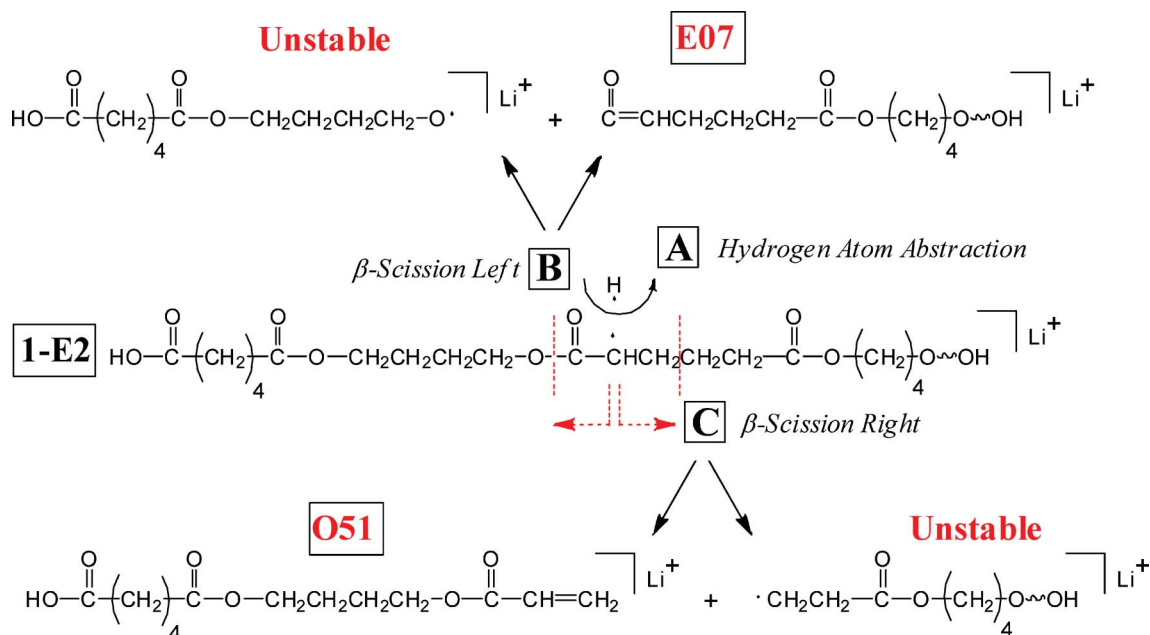


Species (Precursor Ions)	Terminal Groups		Fragment Ion Series			
	T ₁	T ₂	F1 (Li ⁺ /Na ⁺)	F2 (Li ⁺ /Na ⁺)	F3 (Li ⁺ /Na ⁺)	F4 (Li ⁺ /Na ⁺)
Di-Butanol (1-E1)	HO-(CH ₂) ₄ -O-	-(CH ₂) ₄ -OH	E79/E95	E25/E41	E25/E41	E79/E95
Cyclic (1-CyE)	CH ₂ =CH-(CH ₂) ₂ -O-	-H	E61/E77	O53/O69	E07/E23	E07/E23
Butanol-Acid (1-E2)	HO-(CH ₂) ₄ -O-	-H	E79/E95	O53/O69	E25/E41	E07/E23
Di-Acid (1-E3)	HO-	-H	E07/E23	O53/O69	O53/O69	E07/E23
Butanol-Glycol (1-E4)	HO-(CH ₂) ₄ -O-	-(CH ₂) ₂ -OH	E79/E95	O97/E13	E25/E41	E51/E67

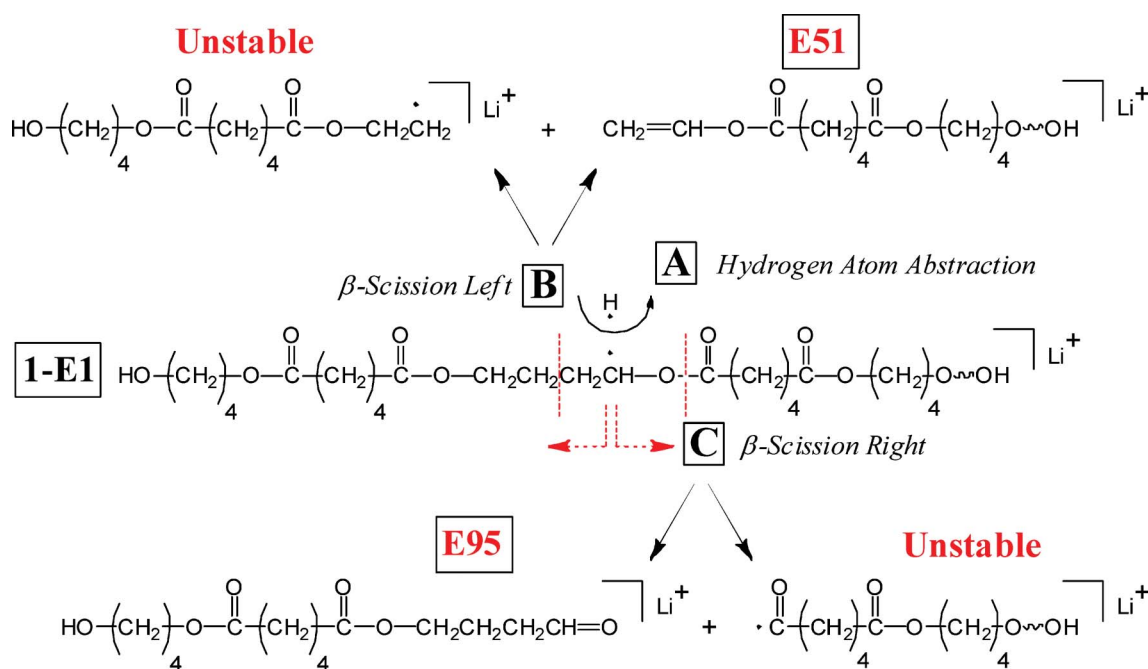
Scheme 1 Major CID fragmentation reactions for poly(butylene adipate) oligomers. 1,5 Hydrogen transfer is the major reaction. Four fragments (F1–F4) are possible; the fragment series listed on the left are for lithium cationized oligomers, those on the right are for sodium cationization. The end groups (T1 and T2) determine the series.



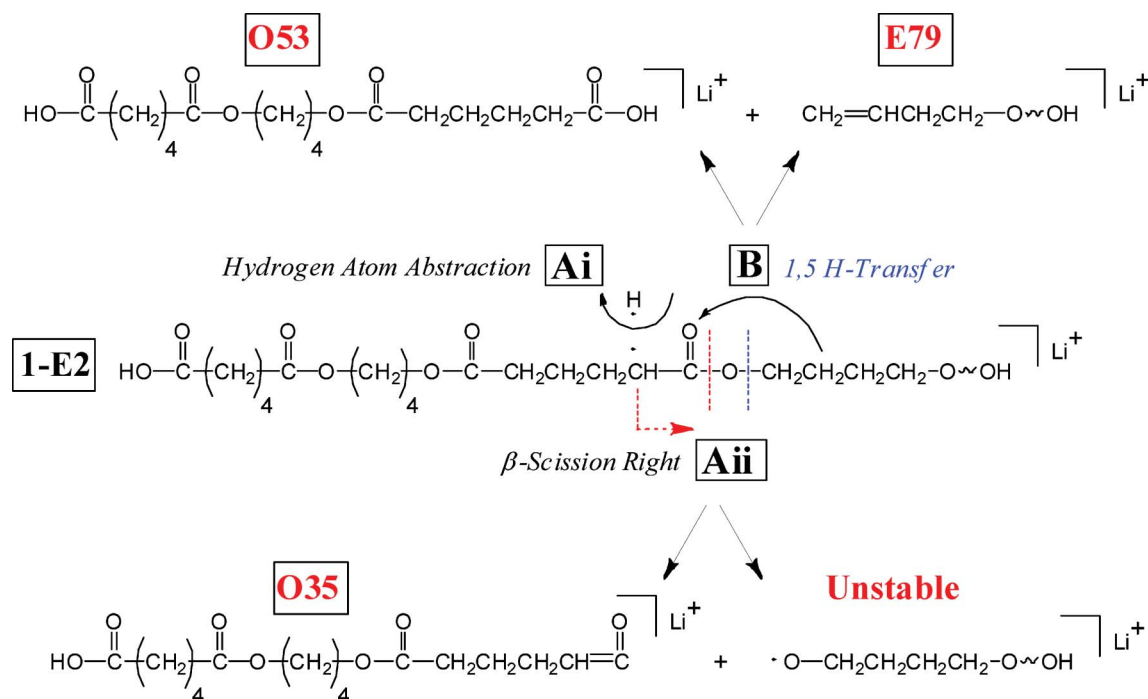
Scheme 2 1,3 Hydrogen shift fragmentation reactions for poly(butylene adipate) oligomers. 1,3 Hydrogen transfer produces two stable fragment series.



Scheme 3 Remote hydrogen abstraction fragmentation reactions—for acid chain α-methylene hydrogens. The structure in the center is the radical produced from hydrogen abstraction by a remote carbonyl group. Each fragmentation produces one stable and one unstable species.



Scheme 4 Remote hydrogen abstraction reactions—for diol chain α -methylene hydrogens the structure in the center is the radical produced from hydrogen abstraction by a remote carbonyl group. Each fragmentation produces one stable and one unstable species.



Scheme 5 Multiple fragmentation reactions for poly(butylene adipate) oligomers. The center species has already undergone an initial 1,5 H-transfer to produce a carboxyl end group. Series O53 is produced by a second 1,5 H-transfer and series O35 by a remote α -H acid abstraction.

different intensities observed between the Li- and Na-cationized spectra. Conversely, the Li-cationized MS/MS species generally will be produced by fragmentation remote from the charge site. A similar effect has been noted recently for acrylic polymers.¹⁴

The relative intensities of the species observed in the present study differ significantly from those reported earlier by Rizzarelli *et al.*¹ Four major series of sodiated fragment ions were reported

by these authors, E41 (Li: E25), E95 (Li: E79), O11 (Li: E95) and O67 (Li: O51). The numbers in parentheses are the lithiated analogs shown in our spectra; all numbers given below will refer to the lithiated species. The two most intense series in their spectra are E95 and O51 while in ours they are E25 and E79. This cannot be due to differing Li and Na cationizing efficiencies; the same series are dominant in both Li and Na

Table 4 Relative ion currents for the MS/MS spectra of PBA oligomers 1-E1 through 1-E4 and Cyclics (1-CyE)

Di-butanol (1-E1)		Cyclic (1-CyE)			Acid-butanol (1-E2)			Di-acid (1-E3)			Butanol-glycol (1-E4)		
%TIC	Mechanism	Frag	%TIC	Mechanism	Frag	%TIC	Mechanism	Frag	%TIC	Mech	Frag	%TIC	Mechanism
38.5	15H	E07	33.6	15H	O53	21.0	15H	E07	29.7	15H	E25	24.9	15H
27.7	15H	O53	24.8	15H	E79	19.6	15H	O53	24.3	15H	E51	18.4	15H
12.8	α HA	O35	15.4	13H, α HA	E07	19.5	15H	E25	17.7	13H	O97	14.9	15H
9.9	α HD	E61	10.1	15H	E25	15.8	15H	E79	13.5	α HA	E07	11.5	13H, α HA
5.9	α HA	E25	6.8	13H	E95	5.2	α HD	O35	9.4	13H	O53	11.0	15H,15H
3.9	15H,15H	E79	6.1	13H, α HA	O35	5.1	13H, α HA	E97	5.4	13H	E79	8.7	15H
1.3	15H, α HA	O89	3.2	13HA	E23	4.9	α HD				O51	4.2	α HA
					O51	4.6	α HA				E95	3.3	α HD
					E97	2.3	13H				O23	1.1	α HA
					O79	2.0	α HD				O79	1.0	13H, α HA
											E67	1.0	α HD

Table 5 Peak series predicted for PBA oligomers 1-E1 through 1-E4 and Cyclics (1-CyE) for acid and diol α -hydrogen abstraction reactions and 1,3 H-shifts. Series listed in "red" are *not* observed in the spectra. Series in "black" are observed. An asterisk (*) indicates coincidence with the 1,5-H shift for that species

Precursor species	Fragmentation mechanism	Lithium cationized fragment peaks predicted for α -H acid abstraction					
1-E1	α H-acid 1,3 H-shift	E07	O51				
1-CyE	α H-acid 1,3 H-shift	E79	O33	O35	O89	E97	
1-E2	α H-acid 1,3 H-shift	E79		O35	O89	E25	
1-E3	α H-acid 1,3 H-shift	E07*	E79*	O35	O51	E25*	E97
1-E4	α H-acid 1,3 H-shift	E79	O35	O35		E25	
1-E4	α H-acid 1,3 H-shift	E07	O23	O51	O79	E69	E97
1-E4	α H-acid 1,3 H-shift	E07			O79		
Precursor Species	Fragmentation mechanism	Lithium cationized fragment peaks predicted for α-H diol abstraction					
1-E1	α H-Diol	E51	E95				
1-CyE	α H-Diol	E23	E33	E77	O79		
1-E2	α H-Diol	E23	E51	E95	O79		
1-E3	α H-Diol	E23	O79				
1-E4	α H-Diol	E23	E51*	E67	E95		

spectra as seen in Fig. 2. We believe that this difference arises from the different acceleration voltages used to obtain MS/MS, 2 kV in their spectra and 1 kV in ours. We were able to increase the intensities of the E95 and O51 series relative to E25 and E79 by increasing the MS/MS acceleration voltage for the CID process. While the earlier spectra offer excellent PBA fingerprints, they do not allow identification of the lowest energy fragmentation pathway in the MS/MS of polyesters.

Cyclic PBA precursor (CyE)—Fig. 6 shows a segment of the MALDI-TOF/TOF CID spectrum for the lithiated cyclic PBA oligomer (1-CyE) with $n = 5$ (1007.5 Da). The precursor ion was selected from the MALDI spectrum shown in Fig. 1B. Fragmentation of cyclic oligomers can be considered (formally) as a two-step process. The first step breaks a bond to open the ring, yielding a species having exactly the same mass as the precursor. The second step leads to subsequent fragmentation; in reality, these probably occur as concerted reactions. The major ring-opening reaction in 1-CyE oligomers is a 1,5 H-shift (*vide infra*) as shown in Scheme 6. Reaction 6A shows transfer of a hydrogen atom to an acid carbonyl, producing a bi-radical, and Reaction 6B yields a species that has olefin and carboxylic acid end groups; this is the species that formally undergoes subsequent fragmentation. Fig. 6 shows that there are three major fragment peak series in the spectrum, E07, E61, and O53. These correspond to the three species predicted by the reaction

shown in Scheme 1 for the cyclic-derived olefin-acid terminated species produced by a 1,5 H-shift ring opening: F1 = E61, F2 = O53 and F3 = F4 = E07. The fact that the E07 intensity in Fig. 6 is approximately the sum of the other two is consistent with the proposed mechanism. So, one can conclude that the major species are produced by two 1,5 hydrogen shifts.

Table 4 lists the %TIC for the seven 1-CyE fragments having %TIC > 1 for $n = 4-8$. The three fragments produced by a 1,5 H-shift account for nearly 69% of the total intensity (33.6% + 24.8% + 10.1% = 68.5%). Table 5 lists the peaks predicted for cyclic oligomers by the 1,3 H-shift and α -hydrogen abstraction mechanisms. The E79, O35 and O89 series are predicted by both mechanisms. The E25 series is predicted uniquely for a 1,3 H-shift and is observed; the O33 series is predicted only for α -hydrogen abstraction, but is not seen. Also, all four peaks predicted for diol α -hydrogen abstraction are not observed. So, species produced involving a 1,3 H-shift are more prominent for cyclic PBA than for the Species 1-E1 linear oligomers. One must remember that it requires two reactions to observe MS/MS fragments for 1-CyE, so the 1,3-H shift could result from either the initial ring opening or subsequent to a 1,5 H-shift ring opening. Given the lack of documented α -hydrogen shifts for 1-CyE tends to support 1,3-H ring opening; this would be minor relative to the 1,5-H ring opening. Another complicating factor in interpreting cyclic MS/MS spectra is that the signal-to-noise

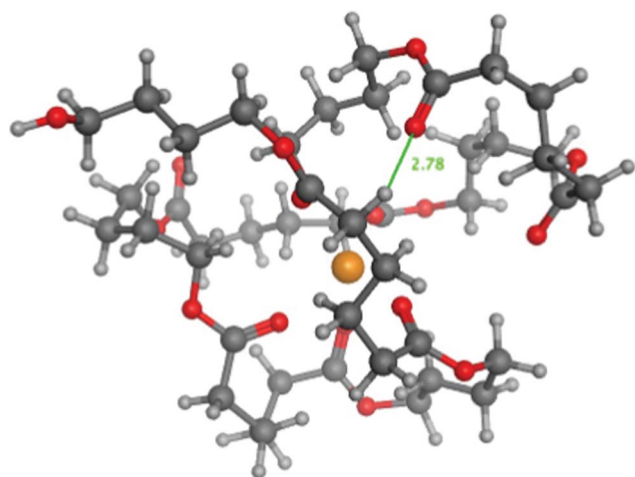


Fig. 3 Representative structure for dibutanol terminated PBA structure 1-E1 ($n = 4$) with sodium cationization. Each atom has been color coded: (1) yellow = sodium ion, (2) red = oxygen atoms, (3) black = foreground carbon atoms, (4) large gray = background carbon atoms, and (5) small gray = hydrogen atoms. The green line shows the close approach of carbonyl and methylene groups (2.78 Å).

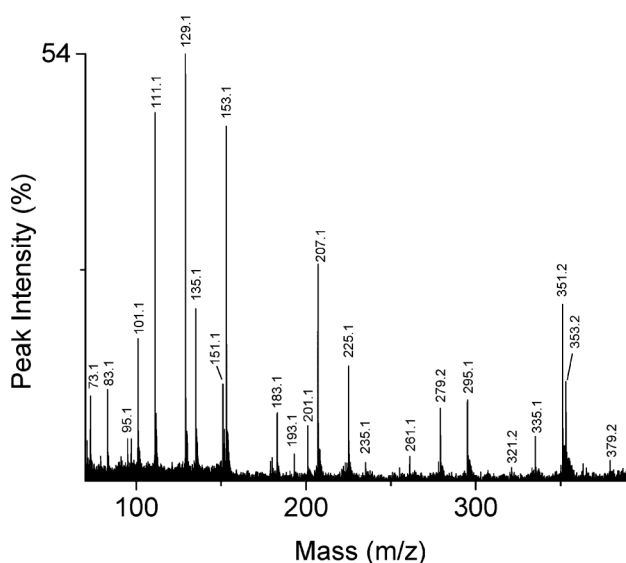
ratio in these spectra is not as good as for spectra where only a single fragmentation is required. One thing for certain is that interpretation of cyclic MS/MS spectra based on the linear acidene structure of Scheme 6 is valid. The peak at 935.5 Da in Fig. 6 corresponds to loss of mass 72 Da, a 3-buten-1-ol fragment.

Butanol-carboxyl PBA precursor (1-E2)—Fig. 7 shows a segment of the MALDI-TOF/TOF CID spectrum for the lithiated linear butanol-carboxyl terminated PBA oligomer (Species 1-E2) with $n = 5$ (1025.5 Da). The precursor ion was selected from the MALDI spectrum shown in Fig. 1B. Fig. 7 shows the presence of four intense series of peaks: E07, E25, E79 and O53. These are the same series predicted on the basis of Scheme 1 for Species 1-E2 oligomers. All are produced by 1,5 H-shift reactions and are characteristic of the Species 1-E2 end groups. Table 4 summarizes the %TIC for the ten fragment ions of the Species 1-E2 oligomers having %TIC > 1 for $n = 4$ –9. The four species listed above have nearly equal intensities, consistent with Scheme 1, and account for approximately 76% of the total ion current (19.5% + 15.8% + 19.6% + 21.0% = 75.9%).

The other peaks listed in Table 4 can be explained by the predictions in Table 5 for 1,3 H-shift and remote site α -hydrogen abstraction reactions. Of the four spectral series predicted for acid α -hydrogen loss, two are coincident with series produced by 1,5 H-shifts (E07, E79). The other two predicted are O35 and O51; both are observed. The O35 series is also predicted for 1,3 H-shift, and the E25 series predicted is coincident with a 1,5 H-shift reaction (E25). However, the E97 series is unique to 1,3 H-shift and is observed. Of the four series predicted uniquely for α -hydrogen abstraction from the diol segment, three are observed: E23, E95 and O79. The E51 series is not seen.

Di-carboxyl PBA precursor (1-E3)—Fig. 8 shows the MALDI-TOF/TOF CID spectrum for the lithiated linear di-carboxyl terminated PBA oligomer (Species 1-E3) with $n = 3$ (753.4 Da). The precursor ion was selected from the MALDI

A. High KE: Monomeric Region
Peak Intensity (129.1 Da) = 54 % of Base Peak



B. High KE: Dimeric/Trimer Region
Peak Intensity (625.3 Da) = 64 % of Base Peak

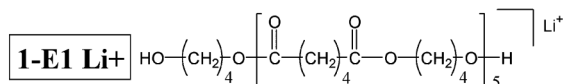
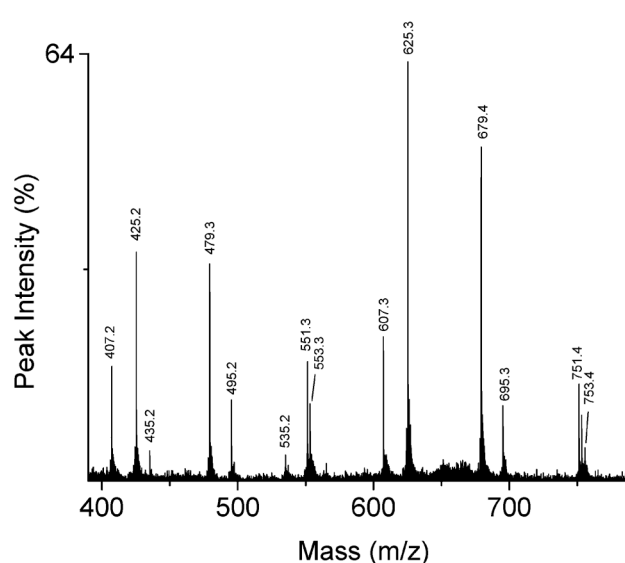
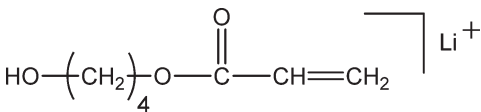
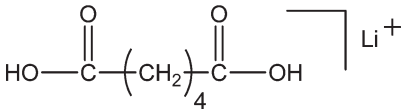
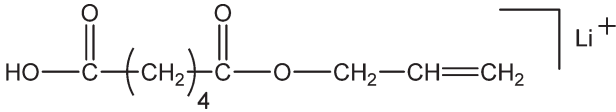
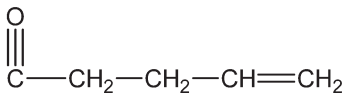
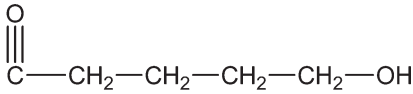
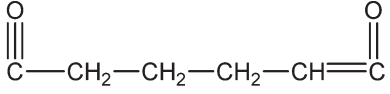
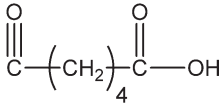
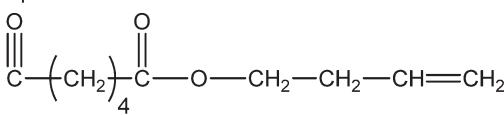
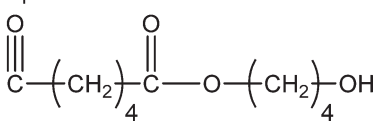


Fig. 4 High effective kinetic energy (collision gas pressure: 1.5×10^{-6} Torr) MALDI-TOF/TOF mass spectrum of dibutanol terminated poly(butylene adipate) (Str. 1-E1 Li^+ , 1097.6 Da); covering the monomeric (A: 70–390 Da) and dimeric through trimeric (B: 390–790 Da) mass regions.

Table 6 Low mass fragments observed in lithium cationized poly(butylene adipate) MS/MS spectra

$(M + Li)^+$ (Da)	Lithium cationized fragment structure (M)
151	
153	
193	
M^+ (Da)	Fragments having intrinsic charge (M)
73	$\bullet+$ $O-CH_2-CH_2-CH_2-CH_3$
83	$\bullet+$ 
101	$\bullet+$ 
111	$\bullet+$ 
129	$\bullet+$ 
183	$\bullet+$ 
201	$\bullet+$ 

spectrum shown in Fig. 1B. Fig. 8 shows the presence of two intense series of peaks: E07, and O53. These are the series predicted on the basis of Scheme 1 for Species 1-E3 oligomers. Both are produced by 1,5 H-shift reactions and are characteristic of the 1-E3 carboxyl end groups; only two series are observed because of molecular symmetry. Table 4 summarizes the %TIC for fragment ions of the Species 1-E3 oligomers having %TIC > 1 for $n = 3-5$. The two peaks from 1,5 H-shift account for 54% of

the TIC (29.7% + 24.3% = 54%). The small number of oligomers and fragments observed for Species 1-E3 reflects the weak intensities of the 1-E3 peaks and therefore poor signal-to-noise ratios.

Three of the other four peaks listed in Table 4 can be explained on the basis of those predicted in Table 5. The E79 and O35 series are predicted for remote acid α -hydrogen abstraction and the E25 and O35 series are predicted for the 1,3 H-shift

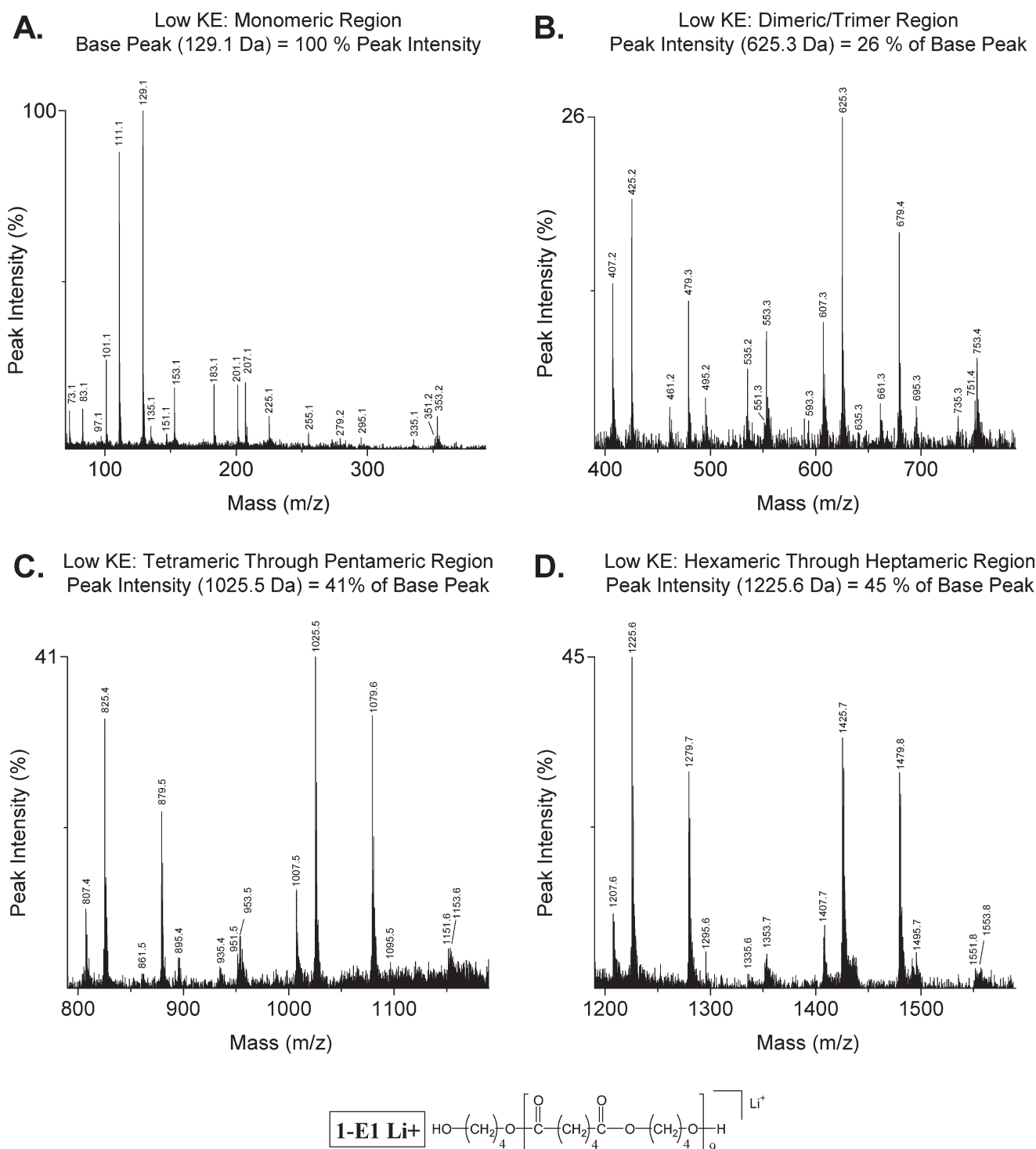


Fig. 5 Low effective kinetic energy (collision gas pressure: 1.5×10^{-6} Torr) MALDI-TOF/TOF mass spectrum of dibutanol terminated poly(butylene adipate) (Str. 1-E1 Li⁺, 1898.0 Da); covering the monomeric (A: 70–390 Da), dimeric through trimeric (B: 390–790 Da), tetrameric through pentameric (C: 790–1190 Da), and hexameric through heptameric (D: 1190–1590 Da) mass regions.

mechanism. Given that the two unique peaks for these series are observed, both mechanisms must be operative. The E23 and O79 series predicted for diol α -hydrogen abstraction are not seen. The E97 series is produced by two 1,3 H-shifts from an acid to a diol oxygen, producing a dihydroxyl terminated species. It is interesting that 1,3 H-shift reactions seem to be more prevalent

for acid-terminated oligomers than for those having only diol terminal groups.

Butanol-glycol PBA precursor (1-E4)—Fig. 9 shows the MALDI-TOF/TOF CID spectrum for the lithiated butanol-glycol end-capped PBA oligomer (Species 1-E4) with $n = 5$ (1069.6 Da). The precursor ion was selected from the MALDI

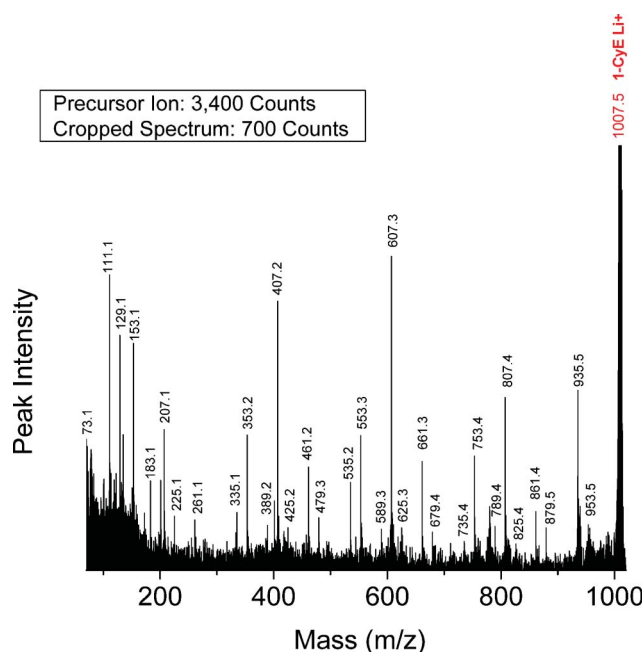


Fig. 6 MALDI-TOF/TOF mass spectrum segment for cyclic PBA structure 1-CyE at a low collision gas pressure of 1.5×10^{-6} Torr. Precursor ion (1007.5 Da) is cationized by lithium.

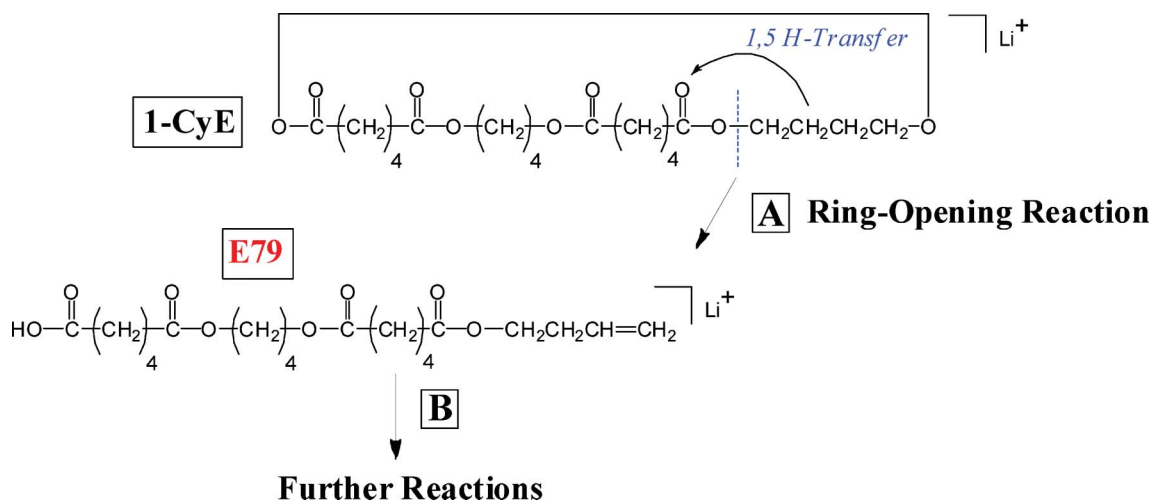
spectrum shown in Fig. 1B. Fig. 9 shows the presence of four intense series of peaks: E25, E51, O97, and E79; they account for approximately 67% of the TIC (24.9% + 18.4% + 14.9% + 8.7% = 66.9%). These are the series predicted on the basis of Scheme 1 for Species 1-E4 oligomers. All four are produced by 1,5 H-shift reactions and are characteristic of the Species 1-E4 hydroxyl end groups; fragments with four end group possibilities are observed because the 1-E4 oligomers are not symmetrical.

Table 4 summarizes the %TIC for fragment ions of the 1-E4 oligomers having %TIC > 1 for $n = 4-8$. Two peak series other than those for 1,5 H-shifts show significant intensities, E07 and O53. Table 5 indicates that the E07 and O79 series are common to the α -hydrogen abstraction and 1,3 H-shift mechanisms. The

presence (although weak) of the O23 and O51 series confirms that the remote α -hydrogen abstraction mechanism occurs in the MS/MS of Species 1-E4. The two unique spectral series predicted for a 1,3 H-shift (E69, E97) are not seen. This suggests that, similarly to 1-E2 oligomers, the 1,3 H-shift is not as important for Species 1-E4 as it is for the acid-terminated oligomers. Three series characteristic of α -hydrogen abstraction from the diol segment occur, but one (E51) is coincident with the 1,5 H-shift. Two unique series for the α -hydrogen diol abstraction are observed, E67 and E95, but one is not, E23. Thus α -H abstraction from the diol is considered to be a minor pathway. The O53 series is produced by two consecutive 1,5 H-shifts as shown in Scheme 5 and is for a fragment species containing two butanediol groups. A similar series containing a glycol group produced by two 1,5 H-shifts would be an O25 series, which is not seen in the spectra. This provides a strong indication that the glycol group is terminal on 1-E4 oligomers, given that fragments F2 and F4 in Scheme 1 (O97, E51) are quite strong and require the inclusion of a glycol group.

An interesting question that has not been addressed so far is whether the MS/MS process can produce a cyclic ester fragment series. Such might be expected, given the “balled-up” structure of PBA oligomers shown in Fig. 3. These species have been reported recently in the MS/MS of a sodiated PBA trimer using a Q/ToF mass spectrometer.¹⁵ The fragment series produced by such a process would be E07. An E07 series is observed in the MS/MS of all oligomers and can be attributed to either 1,5-H abstraction (Species 1-CyE, 1-E2, and 1-E3) or α -hydrogen abstraction from the acid (Species E1 and E4), making the situation somewhat ambiguous. In the case of Species 1-E4 oligomers, a glycol group in the cyclic species would give an O79 series that is observed, albeit weakly. But as described above, it is quite probable that the glycol group is terminal and therefore would be lost in the cyclization reaction if it occurs.

Minor PBA species (1-E5 through 1-E8)—Table 1 and 7 list four minor species (1-E5 through 1-E8) observed in PBA MALDI spectra that account for 1–4% TIC. Plausible structures for these are given in Table 1 and 7. As indicated earlier, the most probable explanation for these species is that they are



Scheme 6 Ring-opening reaction for cyclic oligomers of poly(butylene adipate) by a 1,5 H-transfer reaction. An initial bi-radical is produced (A) and ring opens (B) to give the olefin-carboxyl terminated oligomer that further fragments.

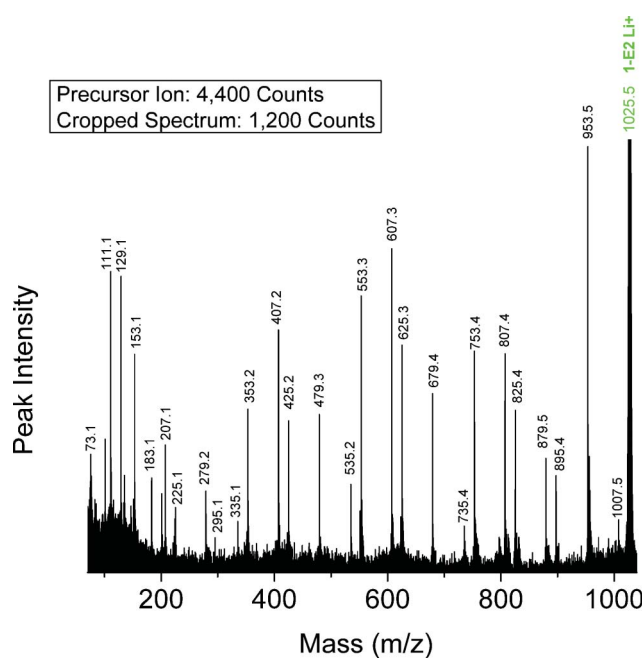


Fig. 7 MALDI-TOF/TOF mass spectrum segment for linear butanol-carboxyl terminated PBA structure 1-E2 at a *low* collision gas pressure of 1.5×10^{-6} Torr. Precursor ion (1025.5 Da) is cationized by lithium.

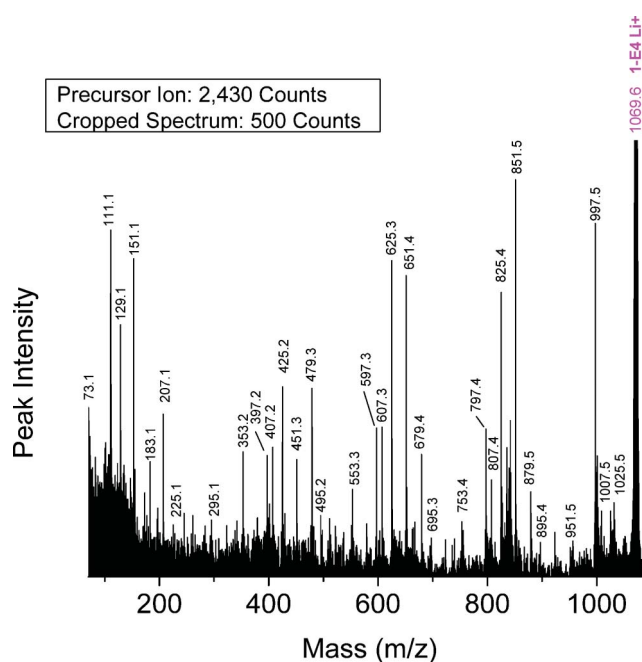


Fig. 9 MALDI-TOF/TOF mass spectrum segment for linear butanol-ethanol terminated PBA structure 1-E4 at a *low* collision gas pressure of 1.5×10^{-6} Torr. Precursor ion (1069.6 Da) is cationized by lithium.

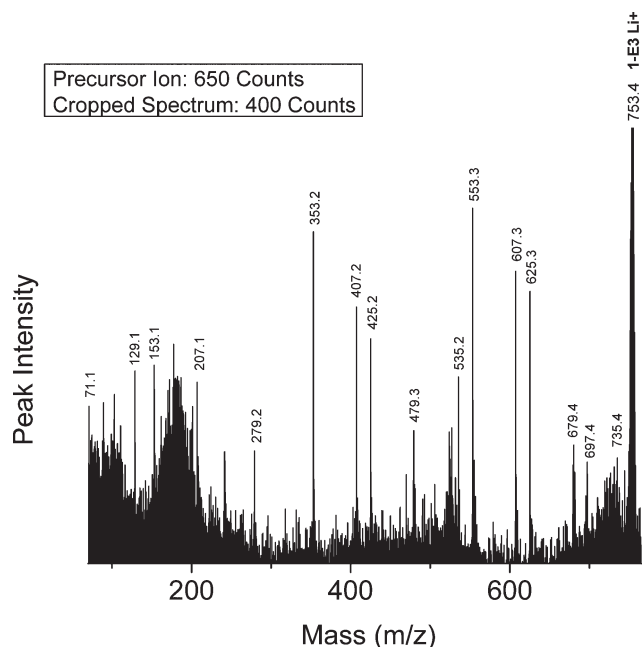


Fig. 8 MALDI-TOF/TOF mass spectrum segment for linear dicarboxyl PBA structure 1-E3 at a *low* collision gas pressure of 1.5×10^{-6} Torr. Precursor ion (753.4 Da) is cationized by lithium.

MALDI artifacts rather than synthesis products. Because they have intensities that allow MS/MS data to be obtained, the structures given in Table 1 are consistent with the MS/MS data, although it requires considerable imagination as to how these might be formed during synthesis.

Table 7 summarizes the MS/MS data for these four species. Based on the behavior of the other PBA oligomers, we assumed

that 1,5-H shift reactions are responsible for the major species in these oligomers. Table 7 lists the spectral series that should be formed for fragments F1–F4 in Scheme 1 for each oligomer. Those in “black type” are spectral series that are observed in the MS/MS spectra of the 1-E5 through 1-E8 “oligomers.” The entry in “red” (e.g., F4 for 1-E5) is not observed, and the entry in “red italics” (e.g., F2 for 1-E5) is seen only weakly. An important point is that E25 and E79 spectral series are observed for all oligomers and these are characteristic of a terminal butanediol group (mass = 89 Da). For this reason all of the structures drawn in Table 7 have been given a butanol group as terminal. This makes it possible to figure the mass of the second terminal group for each oligomer, listed in the table as T₂. The T₂ values are confirmed for the F2 and F4 fragments observed for Species 1-E6 through 1-E8. The reason for questionably observing F2 and F4 (at best) for Species 1-E5 is not clear, but the weak E95 series coupled with the E25 and E79 series does not give rise to reasonable alternatives.

While it might seem that the T₂ end groups in Table 1 and 7 are arbitrarily chosen, there is a limited set of combinations containing only C, H, and O that can fit the data. For Species 1-E5, T₂ must be attached to a diol oxygen so C₄H₇O is the only reasonable combination of elements, a carbonyl followed by a propyl group is the only one that makes sense. Similarly for Species 1-E6, T₂ must be attached to a carbonyl oxygen; C₄H₇ is the only reasonable combination. This could be the olefin as shown in Table 7, or a tetrahydrofuran ring. The olefin could easily be produced from Species 1-E1 by loss of water (either in MALDI or the synthesis). In Species 1-E7, T₂ must be attached to a diol oxygen and have a mass of 29 Da; a carbonyl seems to be more probable than an ethyl group. Finally, for Species 1-E8 a mass of 15 Da is required, meaning a methyl group, although it is hard to see how this attachment could occur. If one allows for

Table 7 Summary of 1,5 H-shift series produced for PBA oligomers 1-E5 through 1-E8. Series in “*italics*” are weak and the other “**bold**” series are *not* observed

Precursor species	Fragment series				Endgroup (T ₂)	Structure (M)
	F1	F2	F3	F4		
1-E5	E79	<i>E95</i>	E25	O49	71 Da	
1-E6	E79	E07	E25	E61	55 Da	
1-E7	E79	E53	E25	O07	29 Da	

the possible inclusion of a glycol in the chain, this would allow end groups of C₃H₅O for Species E7 and C₂H₃O for Species 1-E8. By analogy to Species 1-E5, this would correspond to end groups consisting of a carbonyl and an alkyl group produced from the acid.

Conclusions

MALDI-TOF/TOF CID fragmentation spectra of sodium and lithium cationized poly(butylene adipate) precursor ions were initially examined to determine which cationization agent produced MS/MS data with the best S/N ratios and greatest sequence coverage of PBA oligomers—lithium proved to be the superior for PBA characterization. Additionally, low kinetic energy CID conditions were shown to yield the most reliable data for elucidating PBA fragmentation pathways, especially for studying the degradation processes of the aged samples used in this study. MS/MS data indicate that PBA oligomers undergo a number of low energy degradation pathways: (1) 1,5-H transfer reactions (preferred), (2) 1,3-H transfer, (3) remote hydrogen abstraction reactions, and (4) multiple combinations of these reactions, if sufficient energy is present. Under high kinetic energy conditions, there is a prevalence of multiple fragmentation reactions occurring in concert to produce “unique” fragment ions, which are not routinely observed under low energy conditions. It should be noted that these high energy conditions complicate the interpretation of CID spectra and PBA degradation pathways.

Acknowledgements

We thank Hartmut Nefzger and Bayer Corporation for preparation of the poly(butylene adipate) samples and for

valuable discussions, Michal Kliman for Fig. 3, and Chevron Phillips Chemical Company, LP, for financial support. We greatly appreciate very valuable discussions with Ned Porter.

References

- P. Rizzarelli, C. Puglisi and G. Montaudo, *Rapid Commun. Mass Spectrom.*, 2006, **20**, 1683–1694.
- R. P. Lattimer, H. Muenster and H. Budzikiewicz, *J. Anal. Appl. Pyrolysis*, 1990, **17**, 237–249.
- H. Ohtani, T. Kimura, K. Okamoto and S. Tsuge, *J. Anal. Appl. Pyrolysis*, 1987, **12**, 115–133.
- H. Sato, M. Furuhashi, D. Yang, H. Ohtani, S. Tsuge, M. Okada, K. Tsunoda and K. Aoi, *Polym. Degrad. Stab.*, 2001, **73**, 327–334.
- S. C. Moldoveanu, *Analytical Pyrolysis of Synthetic Organic Polymers*; Elsevier: New York, 2005.
- T. P. Wampler, *Applied Pyrolysis Handbook*, 2nd ed.; CRC Press: Boca Raton, 2007.
- L. R. H. Cohen, D. M. Hercules, C. G. Karakatsanis and J. N. Rieck, *Macromolecules*, 1995, **28**, 5601–5608.
- A. P. Gies, M. J. Vergne, R. L. Orndorff and D. M. Hercules, *Macromolecules*, 2007, **40**, 7493–7504.
- S. T. Ellison, A. P. Gies, D. M. Hercules and S. L. Morgan, *Macromolecules*, 2009, **42**, 3005–3013.
- A. P. Gies, J. F. Geibel and D. M. Hercules, *Macromolecules*, 2010, **43**, 952–967.
- J. T. Mehl, R. Murgasova, X. Dong and D. M. Hercules, *Anal. Chem.*, 2000, **72**, 2490–2498.
- R. Murgasova, E. L. Brantley, D. M. Hercules and H. Nefzger, *Macromolecules*, 2002, **35**, 8338–8345.
- M. Kliman, A. P. Gies, J. A. McLean, D. M. Hercules, *unpublished studies*, Vanderbilt University, 2010–2011.
- J. Song, A. Memboeuf, R. Heeren, V. Karoly and O. F. van den Brink, *Rapid Commun. Mass Spectrom.*, 2010, **24**, 3214–3216.
- C. Wesdemiotis, N. Solak, M. J. Polce, K. C. Dabney and B. C. Katzenmeyer, *Mass Spectrom. Rev.*, 2011, **30**, 523–559.